Utilities Policy 96 (2025) 102014

Contents lists available at ScienceDirect

Utilities Policy

journal homepage: www.elsevier.com/locate/jup

Full-length article

# Modeling the impact of electric vehicle charging on Lisbon's electricity distribution network

Miguel Mouquinho Cardinha [a], Rui Amaral Lopes [a,b,*], Nuno Amaro [a,b]

[a] School of Science and Technology, NOVA University Lisbon, Portugal
[b] UNINOVA-CTS and LASI, Portugal

ARTICLE INFO

Handling Editor: Janice A. Beecher

*Keywords:*
Energy transition
Electric vehicles
Impacts on the power grid

ABSTRACT

This work proposes a methodology to assess the impact of electric vehicle (EV) charging on Lisbon's electricity distribution network, utilizing real load diagrams by postal code and a genetic algorithm to model the baseline and added EV load at substations. The method enables geographic mapping of EV charging to specific substations. Results show that increased EV charging significantly increases power flow, line overloads, and system losses. A fivefold increase caused some lines to exceed 100 % capacity, while a thirtyfold increase led to peak loads at 223 % and losses rising by up to 274 %. Bus voltage levels remained stable across scenarios.

Nomenclature

| | |
|---|---|
| PC | Postal Code |
| $CO_2$ | Carbon Dioxide |
| GHG | Greenhouse Gases |
| INE | National Statistics Institute |
| $NO_2$ | Nitrogen Dioxide |
| RMSE | Root Mean Square Error |
| TSO | Transmission System Operator |
| EV | Electric vehicle |
| $d$ | Distance between the postal code location and the substation (km) |
| $r$ | Radius of the Earth (km) |
| $\phi_A$ | Latitude of the postal code (rad or °) |
| $\phi_B$ | Latitude of the substation (rad or °) |
| $\lambda_A$ | Longitude of the postal code (rad or °) |
| $\lambda_B$ | Longitude of the substation (rad or °) |
| $P_p(c,t)$ | Weighted active power consumption for postal code $c$ at time $t$ (kW) |
| $P(c,t)$ | Active power consumption in postal code $c$ at time $t$ (kW) |
| w(c) | Weight associated with postal code $c$ |
| $T$ | Period of analysis (h) |
| $P_s(t)$ | Total hourly active power at substation $s$ (kW) |
| $\hat{y}_i$ | Estimated values of the load diagrams (kW) |
| $y_i$ | Real power values (kW) |
| $n$ | Total number of data points |
| $CP_{ij}$ | Percentage of postal code $j$ at substation $i$ (%) |
| $\varepsilon_{ij}$ | Excess or deficit of the sum of the percentages of postal code $j$ across substation $i$ (%) |
| $m$ | Index of the mutated substation |
| $V$ | Set of substations with $CP_{ij} > 0.1$ |

(*continued on next column*)

(*continued*)

| | |
|---|---|
| $\gamma_{ij}$ | Proportion of the $CP_{ij}$ value in substation i relative to the total sum of valid values |
| $CP'_{ij}$ | New value of postal code $j$ in substation $i$ after redistribution (%) |
| $E_r$ | Random value for energy (kWh) |
| $T_r$ | Random value for duration (h) |
| $MPC_{in\ use}(h)$ | Average number of charging stations in use during hour h |
| $P_c(h)$ | Charging power consumed in each hour (kW) |
| $P_{CP}$ | Percentage of charging points in each postal code (%) |
| $P_{CP}(h)$ | Average power consumption of the charging sessions in a given postal code during hour $h$ (kW) |
| α | Temperature coefficient of the material (1/°C or 1/K) |
| $\theta_0$ | Reference temperature (°C or K) |
| $R(\theta_0)$ | Electrical resistance at the reference temperature (Ω) |
| $\theta_1$ | Operating temperature (°C or K) |
| $R(\theta_1)$ | Electrical resistance at the operating temperature (Ω) |

## 1. Introduction

In recent years, the burning of fossil fuels has contributed to alarming levels of emissions, exacerbating the challenges associated with climate change. Various greenhouse gases (GHGs), such as nitrogen dioxide ($NO_2$) and carbon dioxide ($CO_2$), primarily resulting from the combustion of fossil fuels, accounted for 70.9 % of Portugal's total emissions in 2022. In addition, according to data from the National Statistics Institute (INE), fuel consumption in road transport increased by 6.1 %, reaching 5.6 million tons of oil equivalent. Diesel contributed to 78.0 % of total fuel consumption in Portugal in 2022 (Instituto Nacional de and

* Corresponding author. School of Science and Technology, NOVA University Lisbon, Portugal.
*E-mail address:* rm.lopes@fct.unl.pt (R.A. Lopes).

https://doi.org/10.1016/j.jup.2025.102014
Received 11 November 2024; Received in revised form 16 July 2025; Accepted 16 July 2025
Available online 24 July 2025

**Table 1**
Literature review summary on related works.

| Ref. | Main focus | Method | Data |
|---|---|---|---|
| Y. Li *et al.*, 2024 (Li and Jenn, 2024) | Seasonal effects on transformer aging. | Simulation in MATLAB/ Simulink. | Simulated load profiles and ambient temperature for different seasons. |
| G. A. Abiassaf *et at.*, 2024 (Abiassaf and Arkadan, 2024) | Technical impacts and environmental benefits. | Simulation of island power systems. | Power system and consumption profiles based on realistic system data and simulated EV penetration scenarios. |
| I. Nutkani *et al.*, 2024 (Nutkani et al., 2024) | Impacts of EVs and distributed storage. | Distribution grid simulation using GridLAB-D software. | Realistic distribution network models and load profiles with simulated charging profiles. |
| B. Williams *et al.*, 2024 (Williams et al., 2024) | Effects of EVs on a small distribution grid. | Power flow simulation. | Realistic university campus network data with load profiles and simulated EV charging profiles. |
| B. V. Kumar *et al.*, 2023 (Kumar and M A, 2023) | Technical impacts of charging stations on the distribution grid. | Review and synthesis of scientific literature. | Secondary data from other scientific articles. |
| F. Daneshzand *et al.*, 2023 (Daneshzand et al., 2023) | Impact of tariff selection in smart charging, grid stress, and carbon reduction. | Simulation of an EV population's charging behavior in response to various tariffs on a low-voltage distribution network. | Real-world driving patterns (from UK National Travel Survey), electricity tariffs, and a representative LV network model, combined with charging decisions (simulated). |
| A. Dall-Orsoletta *et al.*, 2022 (Dall-Orsoletta et al., 2022) | Prospects for EVs and energy transition. | Literature and public policy review. | Secondary data from scientific articles. |
| X. Hu *et al.*, 2021 (Hu et al., 2021) | Impact of EVs on air quality. | Emission inventory modeling (CO, NOx, etc.) using COPERT IV software. | Actual data from vehicle fleet (2014–2018); forecasted scenarios for different EV penetration levels. |
| A.C.R. Teixeira *et al.*, 2018 (Teixeira and Sodré, 2018) | Energy consumption and $CO_2$ emissions. | Life Cycle Analysis (LCA) and emissions calculation. | Statistical data on fuel and electricity consumption and fleet replacement scenarios (forecasts). |
| R. Godina, *et al.*, 2016 (Godina et al., 2016) | Impact of charging on transformers. | Transformer aging simulation. | Actual EV charging profiles measured from 30 users. |
| A. Ul-Haq *et al.*, 2015 (Ul-Haq et al., 2015) | Voltage unbalance. | Simulation of an urban low-voltage distribution network. | Realistic low voltage network with actual load profiles and simulated EV charging profiles. |
| E. Akhavan-Rezai *et al.*, 2021 (Akhavan-Rezai et al., 2012) | Impact of uncoordinated charging. | Power flow simulation on an IEEE 33-bus network. | Standard network data and simulated charging profiles. |
| K. Qian *et al.*, 2011 (Qian et al., 2011) | Modeling EV charging demand. | Stochastic model with Monte Carlo simulation. | National Travel Survey was used to create simulated charging profiles. |
| L. Fernandez *et al.*, 2011 (Pieltain Fernández et al., 2011) | Impact of EVs on distribution networks. | Power flow simulation on realistic network models. | Realistic distribution network data with simulated charging profiles from mobility data. |
| J. A. P. Lopes *et al.*, 2011 (Lopes et al., 2011) | Integration of EVs in the power system. | Comprehensive review of technologies and impacts. | Secondary data from other scientific articles. |
| K. Clement-Nyns *et at.*, 2010 (Clement-Nyns et al., 2010) | Impact of charging on residential grids. | Unbalanced power flow simulation. | Realistic distribution network data, actual household load profiles, and simulated charging profiles. |
| A. S. Masoum *et al.*, 2010 (Masoum et al., 2010) | Impact of charging rates. | Simulation in MATLAB/Simulink on an IEEE 34-bus network. | Network test with actual residential load profiles and simulated charging profiles. |

Estatística, 2023). In this context, there is an increasing need for initiatives that promote the transition to more sustainable energy sources and reduce polluting emissions associated with human activities.

Along with other countries, Portugal has also committed to a green energy transition, recognizing the vital importance of climate issues and the need for a more sustainable approach to achieve an environmentally stable future. Several targets have been proposed, such as those outlined in the National Energy and Climate Plan for the 2021–2030 period, which aims to "*promote the decarbonization of the economy and the energy transition towards carbon neutrality by 2050*" (Portuguesa, 2019). One target is to reduce GHG emissions by at least 40 % by 2030, compared to 1990 levels, as mentioned in the Clean Energy Package for all Europeans (European Commission and Directorate-General for Energy, 2019).

The transition to electric vehicles (EVs) represents a promising approach to achieving these goals and enhancing long-term sustainability by offering an alternative to conventional vehicles. Several studies have observed that the adoption of electric vehicles brings substantial environmental benefits, demonstrating that promoting these vehicles is an effective strategy to reduce emissions from road traffic and improve air quality in urban areas, as they do not emit pollutants (Hu et al., 2021). For instance, according to Teixeira and Sodré (2018), emissions could be 10 to 26 times lower than those of internal combustion vehicles, representing a potential decrease of up to 5600 tons of $CO_2$ per year in Sete Lagoas, Brazil. These results, based on more limited samples, already highlight the effectiveness of electric vehicles in mitigating GHG emissions, suggesting a potentially greater impact if extrapolated to larger scales. According to (Dall-Orsoletta et al., 2022), projections indicate that EVs could reach around 2 billion units by 2050, thereby contributing to the decarbonization of road transport. The European Union has several financial initiatives aimed at encouraging the adoption of electric vehicles. The 2020 report "The European Environment - State and Outlook" identified a series of measures in place to boost the transition to electric vehicles, which are already being implemented in multiple countries, including free charging at public stations, toll exemptions, incentives for manufacturers' sales targets, or the installation of home chargers (European Environment Agency, 2019).

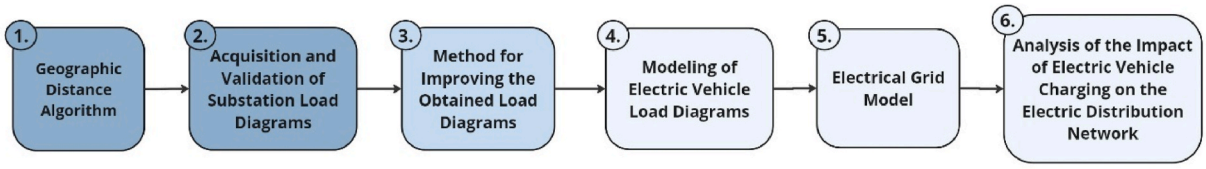


**Fig. 1.** Main phases of the proposed methodology.

However, the expansion of renewable energy sources and the integration of EVs into the electric grid bring several challenges compared to conventional energy distribution and management methods, thereby increasing the complexity of their implementation. Furthermore, the high population concentration in large cities, such as Lisbon, Portugal, might lead to an accumulation of electric vehicle charging in relatively small areas. This situation introduces new uncertainties that can significantly increase pressure on the grid due to simultaneous charging times coinciding with peak consumption hours, increased demand resulting from load growth, voltage drops, and increased losses, among other factors (Kumar and M A, 2023). Challenges can arise not only from the technical aspects mentioned earlier but also from fluctuations in energy prices or the application of inappropriate tariffs for EV charging (Daneshzand et al., 2023).

Several works have addressed the impact of electric vehicle charging on electricity distribution networks. From the analysis of charging loads to assess overloading issues (Akhavan-Rezai et al., 2012), (Qian et al., 2011), (Godina et al., 2016), (Li and Jenn, 2024), or the examination of electric vehicles' effects on distribution losses (Pieltain Fernández et al., 2011), (Clement-Nyns et al., 2010), (Lopes et al., 2011), (Abiassaf and Arkadan, 2024) and voltage stability (Nutkani et al., 2024), (Masoum et al., 2010), (Williams et al., 2024), (Ul-Haq et al., 2015), different examples can be found in the literature. Table 1 provides a summary of the literature review, highlighting the main scientific/technological focus of the research considered.

Whilst most works found in the literature provide sound results on the study of the impact of charging in distribution systems, they mostly do so using open-source grid models or are based on incomplete datasets (e.g., considering synthetic or average load profiles). This work considers the 60 kV portion of the distribution network in the city of Lisbon. The model is constructed using realistic data obtained from the DSO (e.g., line parameters and length). Simulated operational scenarios are also based on realistic assumptions, i.e., considering realistic load profiles for an entire year, with 15-min intervals. This study then focuses on the impact of electric vehicle charging on the electricity distribution network, leveraging real energy consumption data by postal code to design load profiles for each substation. It associates real data on EV consumption with the respective postal codes and corresponding substations. This work proposes a solution for the Lisbon region and others with the availability of similar data that (i) establishes an association between Postal Code (PC) areas and substations, (ii) uses energy consumption data from the Open Data portal of E-REDES (E- REDES), the Portuguese electricity distribution system operator, to develop load profiles for each substation, (iii) generates electric vehicle consumption profiles based on data from the MOBI.E network (MOBI.E), the Electric Mobility Network Managing Entity, associating EV charging power demand with the respective postal codes and substations, and (iv) implements a model to simulate the electrical grid of Lisbon, analyzing the corresponding impacts on the distribution network. Moreover, this methodology can be applied to other distribution networks, provided that equivalent data sources are available.

The remainder of this article is structured as follows: Section 2 details the methodology employed in this study, including the proposed solution, while Section 3 presents the results and corresponding analysis. Finally, Section 4 provides the conclusions and outlines potential directions for future research.

## 2. Methodology

This section describes the proposed solution for assessing the impact of electric vehicle charging on the electricity distribution network in Lisbon and other areas with available data.

The main methodological steps are depicted in Fig. 1. Load diagrams are obtained from the Open Data Portal from E-REDES. This portal provides 15-min timestep load values separated by postal codes (geographic zones in the city). As these are not linked to electrical substations, a dedicated methodology was created to allocate the load diagrams to each substation of the network. This step is described in section 2.1.

The allocation of loads to each substation involves various aspects related to the distribution network structure rather than proximity (as in a geographic criterion, such as postal codes). Thus, this initial process of load allocation was improved through a pro-rata distribution for multiple substations based on their proximity to each postal code, followed by the application of an optimization algorithm to determine the optimal weights for this allocation. The obtained results were compared with reference data obtained from the DSO E-REDES (load profiles from substations). This reference data was not used as the main dataset for load profiles, as it is private data from the DSO. These two steps are described in sections 2.2 and 2.3, respectively.

Section 2.4 focuses on the model developed for EV consumption profiles. Finally, Section 2.5 describes the creation of the simulation model for the Lisbon power grid.

This approach then involves determining the contribution of each postal code (i.e., the electricity consumption associated with each postal code) to the load diagram of its corresponding substation within the Lisbon municipality, using data from the Open Data portal of E-REDES and the geographic distances between postal codes and substations, given that no direct link between the postal codes and the substations has been carried out before. To validate the generated load diagrams, the Root Mean Square Error (RMSE) was calculated by comparing them with the real consumption profiles of the substations. To further improve accuracy, a genetic algorithm-based method was applied (see Subsection 2.3).

### 2.1. Geographic distance algorithm

The main objective of this stage is to determine the proximity between the postal codes available in the Open Data portal of E-REDES, specifically from the dataset "Hourly Consumption by 4-Digit Postal Code", which provides the hourly active energy consumption for the first four digits of each postal code - and the 22 substations of 60 kV located in the municipality of Lisbon. We note that no explicit link is provided between these postal codes, which represent geographic areas defined by the postal service, and the substations supplying the considered area. While this method does not capture the full complexity of the urban distribution network's structure, a proximity-based approach was adopted as an approximation due to the lack of publicly available data linking specific delivery points to substations. Therefore, this geographic distance algorithm aims to associate each postal code belonging to Lisbon with the nearest electrical substation. The process began by accessing an API (JBay Solutions, 2022), which provides the geographic coordinates (latitude and longitude) of the postal codes in Portugal, allowing the retrieval of the full postal code locations associated with

the first four digits available on the portal. Once this information was obtained, the distance between each postal code and the nearest substation was calculated using the Haversine formula in Eq. (1), where $d$ represents the distance between the postal code location and the substation, $r$ is the radius of the Earth, while $\phi_A$, $\phi_B$, $\lambda_A$, and $\lambda_B$ denote the latitudes and longitudes of both the postal code and the substation, respectively, all expressed in radians. The goal is to determine the closest substation to each postal code, thus considering that this substation is responsible for supplying electrical energy to that specific area.

$$d = 2.r.\arcsin\left(\sqrt{\sin^2\left(\frac{\phi_B - \phi_A}{2}\right) + \cos(\phi_A).\cos(\phi_B).\sin^2\left(\frac{\lambda_B - \lambda_A}{2}\right)}\right) \quad (1)$$

However, some uncertainties must be considered, as they may lead to variations in the load diagram results. For instance, data for specific postal codes, such as those related to large private consumers (e.g., airports and shopping centers), are excluded from the portal due to privacy concerns, which may result in an underestimation of the total load in some substations. This underestimation of current load levels can potentially impact the capacity for connecting additional EVs in these substations. Nonetheless, using the methodology presented in this paper, particularly the load adaptation optimization process detailed in Sections 2.2 and 2.3, this effect is less impactful on the obtained results. Furthermore, substations located near the borders of the municipality may exhibit larger errors due to the proximity of external consumption sources that are not considered. The approach used in the geographic distance algorithm also assumes that a postal code is closer to a specific substation, implying it is fed by that substation, which is not necessarily true. This assumption can lead to variations in load distribution, with certain substations potentially appearing to have higher or lower loads than they do. Additionally, there are differences in temporal granularity between the consumption data from the portal and the real load diagrams, which required additional data treatment during validation. Due to the limitations presented here, load diagrams obtained from this method are further enhanced through the application of the optimization process explained in sections 2.2 and 2.3.

### 2.2. Acquisition and validation of substation load diagrams

The weighted active power for each postal code was calculated using Eq. (2), where $P_p(c,t)$ represents the weighted active power consumption for postal code $c$ at time $t$, $P(c,t)$ corresponds to the active power consumption in postal code $c$ at time $t$, obtained from the hourly active energy data for each postal code extracted from the Open Data portal of E-REDES. In this context, the active energy consumption (in kWh) for each postal code associated with the substation is numerically equal to the active power in kW. Additionally, $w(c)$ is the weight associated with postal code $c$ as determined by the geographic distance algorithm, and $T$ represents the period of analysis.

$$P_p(c,t) = P(c,t) \times w(c), \forall_t \in T \quad (2)$$

Subsequently, for each substation $s$ in the set of substations $S$, and for each postal code $c$ in the set of postal codes associated with substation $s$, $C_s$, the weighted consumptions of all postal codes were summed to obtain the total hourly active power $P_s(t)$ at substation $s$ for any time instance $t$ using Eq (3).

$$P_s(t) = \sum_{c \in C_s} P_p(c,t), \forall_t \in T \quad (3)$$

The real load diagrams for the substations have a temporal resolution of 15 min. To compare these with the hourly data obtained from the portal, it was necessary to convert the hourly load profiles to 15-min intervals. Given that the numeric value of the active energy measured in kWh over an hour is numerically equal to the average power in kW during that hour, the average power during each 15-min interval was considered equal to the hourly average power. Thus, each hourly value was replicated four times during a specific hour. To validate the implemented methodology, RMSE was used to compare the accuracy of the load diagrams obtained through the implemented methodology (data from the Open Data portal of E-REDES) with the actual load diagrams of each substation, allowing for the identification of discrepancies resulting from the uncertainties and approximations in the developed model. In Eq. (4), $\hat{y}_i$ represents the estimated values of the load diagrams generated by the model, $y_i$ denotes the real power values, and $n$ is the total number of data points.

$$RMSE = \sqrt{\sum_{i=1}^{n} \frac{(\hat{y}_i - y_i)^2}{n}} \quad (4)$$

### 2.3. Method for improving the substation load diagrams

Due to the multi-objective nature of the proposed model, the study employs a genetic algorithm to optimize the allocation of postal code percentages by substation, considering geographical constraints. The primary objective of the algorithm is to determine the best allocation of postal code percentages by substation, ensuring that the sum of percentages for each postal code is always unitary and that the fitness value does not decrease without compromising the established geographical constraints.

#### 2.3.1. Description of the genetic algorithm components

The solutions are represented by individuals in a population that evolves over generations. Each individual is composed of a series of weights that associate postal codes and substations (e.g., a postal code closer to a substation is weighted more heavily). The algorithm was slightly modified so that each individual is represented by a single chromosome, where each gene corresponds to a pair (postal code, percentage), representing the percentage of a specific postal code associated with a substation. The fitness function is used to evaluate the quality of each solution by assessing the distribution of postal code weights. It is calculated based on the RMSE for each substation, comparing the modeled power data with the actual data. The proposed algorithm was adapted to include only mutations, thereby avoiding other evolutionary operations, such as crossover between individuals, due to geographical constraints. These genetic operations could result in the allocation of postal code percentages to substations that are not geographically related, which would compromise the approach. Mutations are applied to genes representing postal code percentages greater than 0.1, with variations between −0.1 and 0.1. This value was chosen because percentages below 10 % were considered negligible, as they do not significantly impact the total load. It was observed that, for a given solution, a postal code often holds a more significant weight, while others are distributed in a more dispersed manner.

After each mutation, the total sum of the weights assigned to the specific postal code must remain unitary, preventing deviations that could affect the proper distribution of postal code weights. To achieve this, after mutating the gene, any excess or deficit is corrected using Eq. (5), where $\varepsilon_{ij}$ corresponds to the excess or deficit of the sum of the percentages of postal code $j$ across substation $i$ after the mutation, $CP_{ij}$ represents the percentage of postal code $j$ at substation $i$, and $n$ is the total number of substations.

$$\varepsilon_{ij} = \left(\sum_{i=1}^{n} CP_{ij}\right) - 1 \quad (5)$$

Subsequently, the values of the postal code in each substation greater than 0.1 are identified, excluding the substation that underwent the mutation, and the proportion of each associated with the same postal code for each substation relative to the total sum is calculated using Eq. (6). In this equation, $m$ represents the index of the mutated substation, $V$ the set of substations with $CP_{ij} > 0.1$ and $\gamma_{ij}$ refers to the proportion of

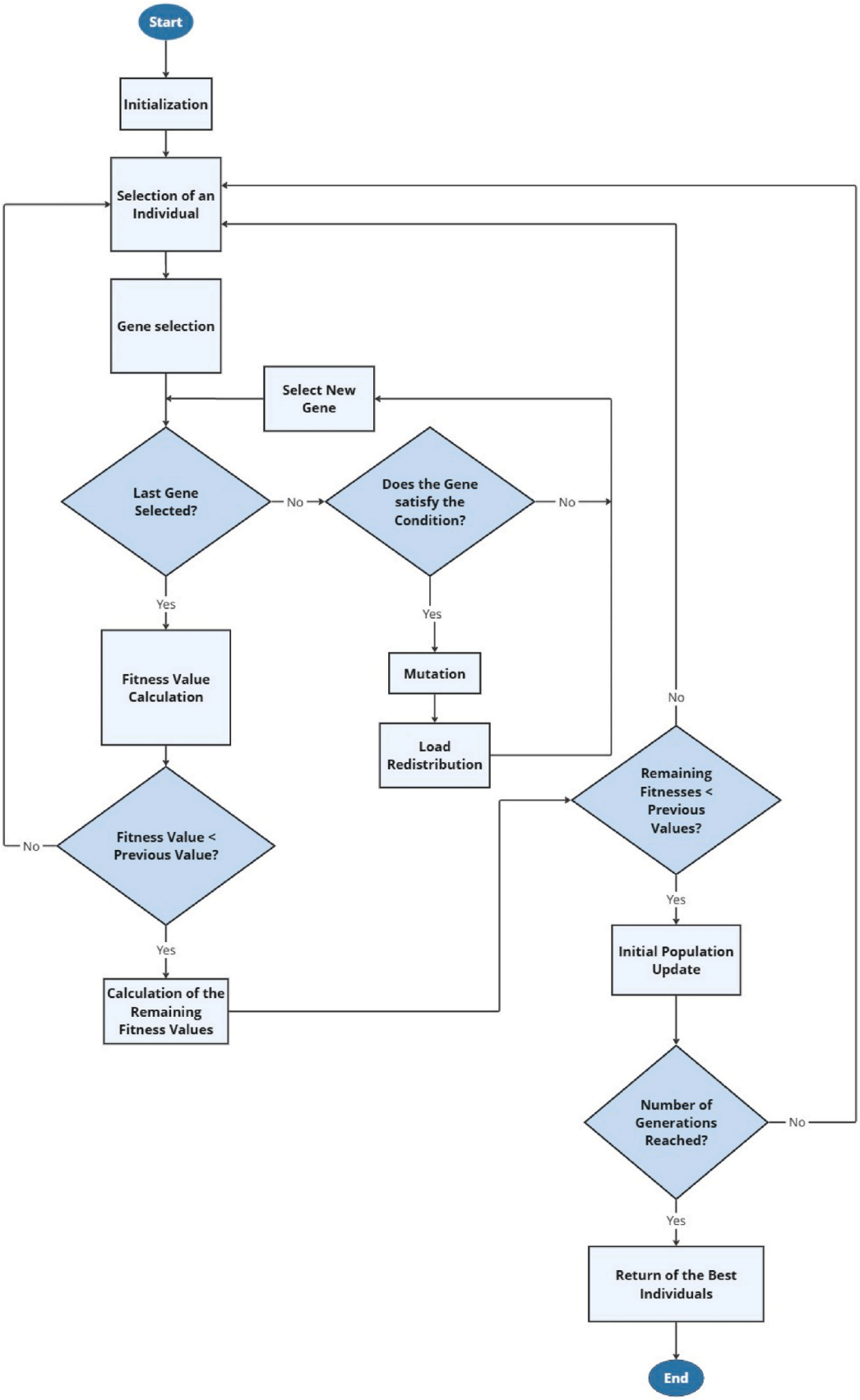


**Fig. 2.** Genetic algorithm flowchart.

**Table 2**
Power grid model generators.

| Generators | Alto São João | Carriche | Sacavém | Sete Rios | Zambujal |
|---|---|---|---|---|---|

the $CP_{ij}$ value in substation $i$ relative to the total sum of valid values.

$$\gamma_{ij} = \frac{CP_{ij}}{\sum_{i \in V} CP_{ij}}, i \neq m \quad (6)$$

The values of the postal codes in the substations are adjusted as necessary, removing excess or adding deficit, to ensure that the final sum is unitary, according to Eq. (7), with $CP'_{ij}$ representing the new value of postal code $j$ in substation $i$ after redistribution.

$$CP'_{ij} = CP_{ij} - \varepsilon_{ij} \times \gamma_{ij} \quad (7)$$

In situations where only one substation has a significant value for a postal code (>0.1), that gene does not undergo mutation, as the solution is considered already satisfactory.

#### 2.3.2. Genetic algorithm initialization parameters

The initial population was randomly generated from the individuals obtained through the geographic distance algorithm, ensuring that each individual appears at least once. A sample of 100 individuals was maintained to ensure adequate diversity. The number of generations was set to 30 after observing that significant improvements occurred up to the 20th generation. Since mutation is the only source of genetic variation applied, different mutation values were tested, and it was found that the best performance was achieved with a unitary mutation rate. The number of generations determined the stopping criterion.

#### 2.3.3. Structure and functioning of the genetic algorithm

The genetic algorithm implemented follows an iterative process, as illustrated in Fig. 2, aimed at evolving towards a satisfactory solution. The algorithm employs elitism, retaining the best individuals from each generation, which helps ensure that the search space does not become excessive and that performance gains are maintained throughout the iterations. The steps that make it up are as follows.

1. Initialization: The initial population is randomly generated from the substations, and postal code weights are obtained using the geographic distance algorithm.
2. Selection of an Individual: An individual is randomly selected from the population.
3. Gene selection: The genes of the selected individual are identified.
4. Gene verification:
   a. If all the genes have already been verified, the algorithm moves on to Step 9.
   b. Otherwise, the process continues to Step 5.
5. Gene evaluation:
   a. If the gene has a postal code percentage greater than 0.1, the algorithm proceeds to Step 7.
   b. Otherwise, the algorithm advances to Step 6.
6. Select New Gene: A new gene is selected. The algorithm returns to Step 4.
7. Mutation: The gene of the selected individual is mutated.
8. Load Redistribution: The weights of the mutated postal codes are adjusted to ensure that the sum remains unity. The algorithm returns to Step 6.
9. Fitness Value Calculation: The individual's fitness value is recalculated to reflect the changes that have occurred.
10. Fitness Value Comparison:
    a. If the new fitness value is better (i.e., lower), the algorithm proceeds to Step 11.
    b. Otherwise, a new individual is selected, and the process returns to Step 2.
11. Calculation of the Remaining Fitness Values: The fitness values of the remaining individuals are recalculated to reflect the changes caused by the mutation.
12. Comparison of the Remaining Fitness Values:
    a. If the recalculated values are better than the previous ones, the algorithm proceeds to the next step.
    b. Otherwise, it returns to Step 2.
13. Initial Population Update: The population is updated with the new individuals and their recalculated fitness values.
14. Stop Criterion Check:
    a. If the maximum number of generations has been reached, the algorithm advances to Step 15.
    b. Otherwise, it returns to Step 2.
15. Return of the Best Individuals: After reaching the maximum number of generations, the algorithm returns the best individuals from the last generation as the improved solution.

### 2.4. Modeling of electric vehicle load diagrams

In this study, data from the MOBI.E portal were used to model the load diagrams of electric vehicles in the Lisbon municipality. MOBI.E provides the location and size (power) of each charging station. The modeling of the charging process was based on a probabilistic model, utilizing average consumption and charging duration values ($E_m$ = 19 kWh and $T_m$ = 2.13 h), with standard deviations of 10 % for both. Random values for energy ($E_r$) and duration ($T_r$) of the charging sessions, defined for each hour of the day, were generated using normal distributions. The charging power consumed in each hour was calculated as presented in Eq. (8), where $MPC_{in\ use}(h)$ represents the average number of charging stations in use during hour h, based on data extracted from the MOBI.E portal.

$$P_c(h) = \frac{E_r \times MPC_{in\ use}(h)}{T_r} \quad (8)$$

Each charging point was associated with its respective postal code, based on its location, which was also provided by the MOBI.E portal. Considering the percentage of charging points per postal code, which represents the relative contribution of each postal code to the total number of charging points in the Lisbon municipality, the average power consumption of the charging sessions in a given postal code during hour $h$, $P_{CP}(h)$, was calculated according to Eq. (9), with $p_{CP}$ representing the percentage of charging points in each postal code.

$$P_{CP}(h) = P_c(h) \times p_{CP} \quad (9)$$

Charging points associated with postal codes that are not included in the E-REDES Open Data portal, as well as those that were out of service or blocked, were removed. Finally, using the active power consumption data by postal code from the electric vehicles (EVs) and the optimized weights of these postal codes obtained through the genetic algorithm, load diagrams for each substation related to EV consumption were created according to the method described in Subsection 2.2. Moreover, this methodology enables the association of EV consumption with substations through postal codes, offering information that is not commonly available.

### 2.5. Electrical grid model

In this study, the modeling of the Lisbon power grid and the power flow analysis are conducted using the PandaPower library in Python (Thurner et al., 2018). For the analysis of EV charging, the Lisbon electrical grid was modeled at the 60 kV level. This model includes five generators, 27 buses, and 56 lines, whose characteristics were obtained from the information provided by E-REDES (E−REDES, 2022). The five modeled generators listed in Table 2 represent the function of

**Table 3**
RMSE (*kW*) comparison across different substations using different algorithms.

| RMSE (kW) | | | | | |
|---|---|---|---|---|---|
| Substation | Geographic Distance Algorithm | Genetic Algorithm Mutation Rate | | | RMSE Reduction (%) |
| | | 50 % | 75 % | 100 % | |
| **Aeroporto** | 13306.13 | 5929.14 | 5653.88 | 5561.10 | 58.21 |
| **Alameda** | 2010.25 | 1360.29 | 1338.04 | 1330.00 | 33.84 |
| **Alto Lumiar** | 2406.81 | 493.57 | 563.51 | 539.88 | 77.57 |
| **Amoreiras** | 3297.38 | 3165.68 | 1581.99 | 1800.77 | 45.39 |
| **Arco Carvalhão** | 2869.96 | 2476.57 | 1227.67 | 1228.89 | 57.18 |
| **Boavista** | 5060.38 | 4833.78 | 1698.90 | 1709.10 | 66.23 |
| **Central Tejo** | 7400.09 | 6349.96 | 6328.45 | 6467.33 | 12.60 |
| **Colombo** | 3048.31 | 1693.09 | 1721.09 | 1775.92 | 41.74 |
| **Entrecampos** | 2688.30 | 1284.96 | 1579.64 | 1917.40 | 28.68 |
| **Expo SUL** | 8023.54 | 2179.83 | 2140.38 | 2258.96 | 71.85 |
| **Gago Coutinho** | 3373.64 | 2014.45 | 1892.17 | 1679.56 | 50.22 |
| **Luz** | 7333.50 | 5019.87 | 4444.93 | 3535.01 | 51.80 |
| **Marvila** | 10406.82 | 8356.58 | 8600.22 | 7708.91 | 25.92 |
| **Norte** | 14071.52 | 14071.52 | 13788.17 | 13305.16 | 5.45 |
| **Parque** | 2226.31 | 1627.07 | 1625.97 | 1682.97 | 24.41 |
| **Praça Figueira** | 2277.60 | 2245.71 | 2248.29 | 2248.36 | 1.28 |
| **Santa Marta** | 6114.69 | 3077.98 | 3677.46 | 4194.52 | 31.40 |
| **São Ciro** | 6315.74 | 4980.17 | 1431.85 | 1377.82 | 78.18 |
| **Senhor Roubado** | 8755.99 | 7781.99 | 7683.34 | 7704.92 | 12.00 |
| **Telheiras** | 3307.75 | 2040.73 | 1621.93 | 1271.40 | 61.56 |
| **Vale Escuro** | 1260.08 | 1122.12 | 1152.24 | 1154.18 | 8.40 |
| **Zambujal** | 10644.74 | 10644.74 | 10644.74 | 10284.72 | 3.38 |
| **Average RMSE** | **5736.34** | **4215.9** | **3756.59** | **3669.86** | **36.02** |

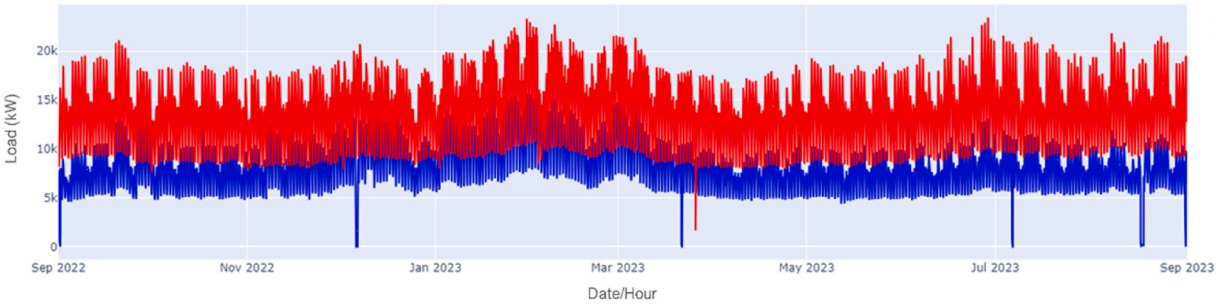


**Fig. 3.** São Ciro substation load diagram. Red line - data from the Open Data portal. Blue line - reference data. (For interpretation of the references to colour in this figure legend, the reader is referred to the Web version of this article.)

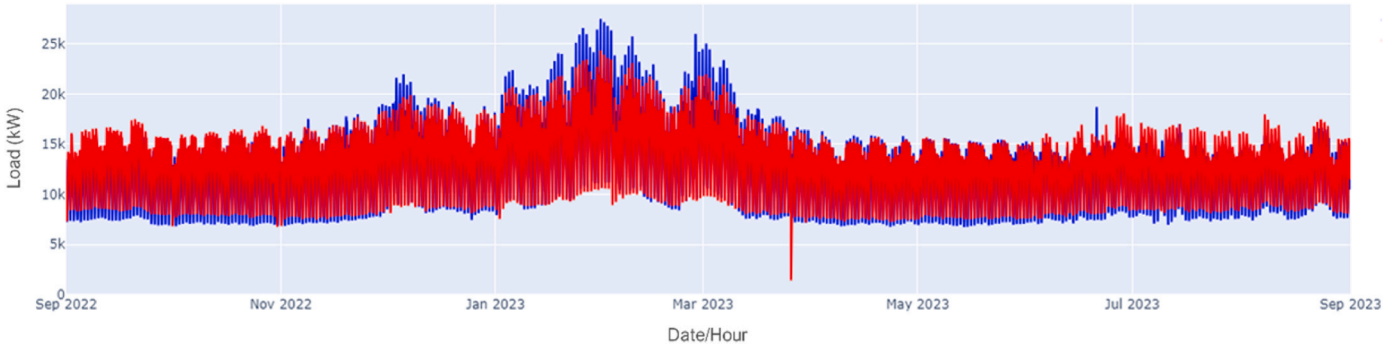


**Fig. 4.** Vale Escuro substation load diagram. Red line - data from the Open Data portal. Blue line - reference data. (For interpretation of the references to colour in this figure legend, the reader is referred to the Web version of this article.)

transmission grid buses, which are responsible for supplying the necessary energy to the distribution network. Therefore, it is assumed that the transmission system acts as an infinite bus, providing the required power for all loads existing in the distribution system. This approach is realistic, as it is based on current real system operation procedures. All generators were configured as slack buses since each interconnection point to the transmission grid must receive the required energy directly from it. Additionally, 27 buses were included in the model (see Table 3), corresponding to substations located within the geographical boundaries of the Lisbon municipality. For modeling purposes, the switching stations were also represented as buses.

For the implementation of the grid, some modifications and

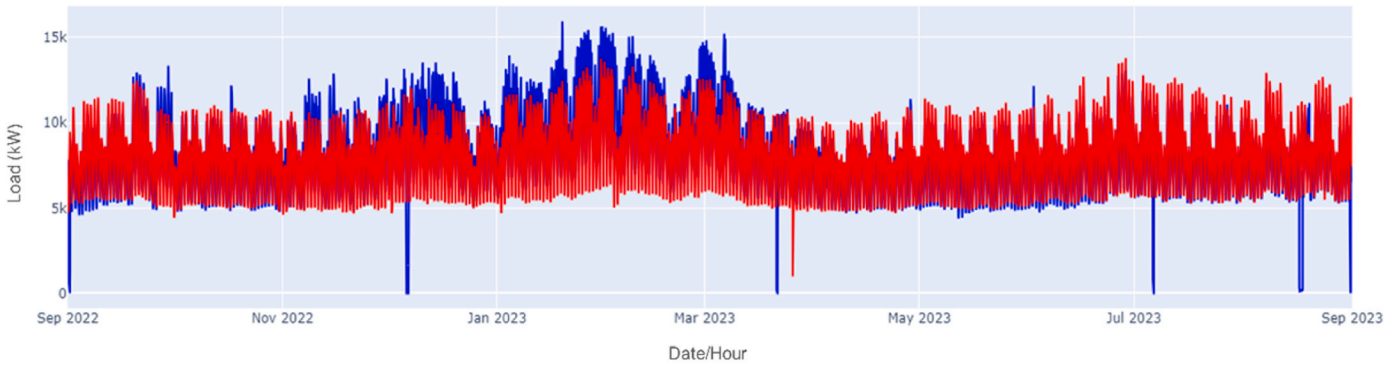


**Fig. 5.** São Ciro substation load diagram after applying the genetic algorithm. The red lines represent data from the Open Data portal; the blue lines represent the reference data. (For interpretation of the references to colour in this figure legend, the reader is referred to the Web version of this article.)

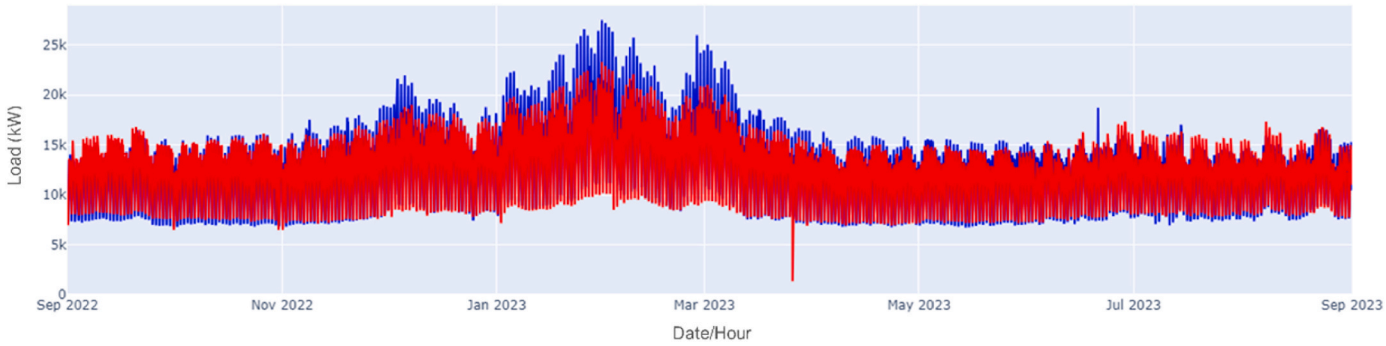


**Fig. 6.** Vale Escuro substation load diagram after applying the genetic algorithm. The red lines represent data from the Open Data portal; the blue lines represent the reference data. (For interpretation of the references to colour in this figure legend, the reader is referred to the Web version of this article.)

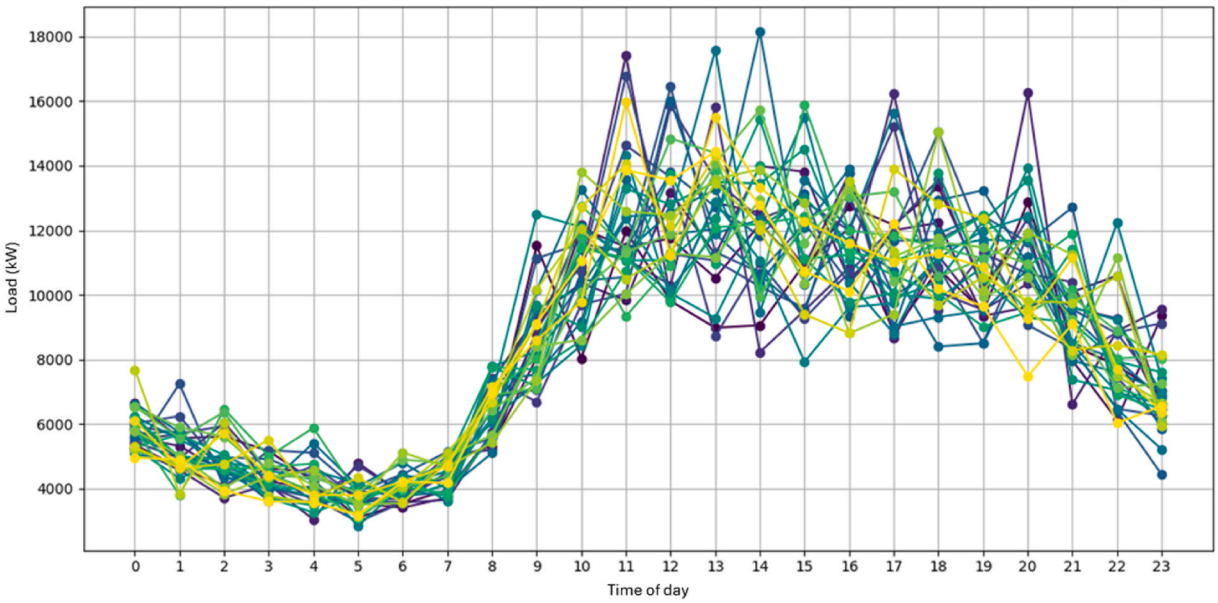


**Fig. 7.** Example of electric vehicle power consumption in a specific month.

considerations were necessary regarding the information provided by E-REDES about the lines. Regarding the physical characteristics, for lines with the same identifier code (i.e., different segments of the same line), only one segment was considered, with the total length determined by the sum of the individual lengths of each segment. In these cases, the cable type and the cross-sectional area corresponding to the longest segment were considered as the dominant features. Additionally, in situations where parallel lines had significantly different lengths, the length was approximated to the one that made the most sense.

The electrical characteristics of the lines in the model include resistance, inductance, capacitance, and maximum supported current. For the AA and AXKJ cables, whose complete specifications were not available, they were assumed to have electrical characteristics similar to those of the LXHIOLE cables of the corresponding cross-sectional area.

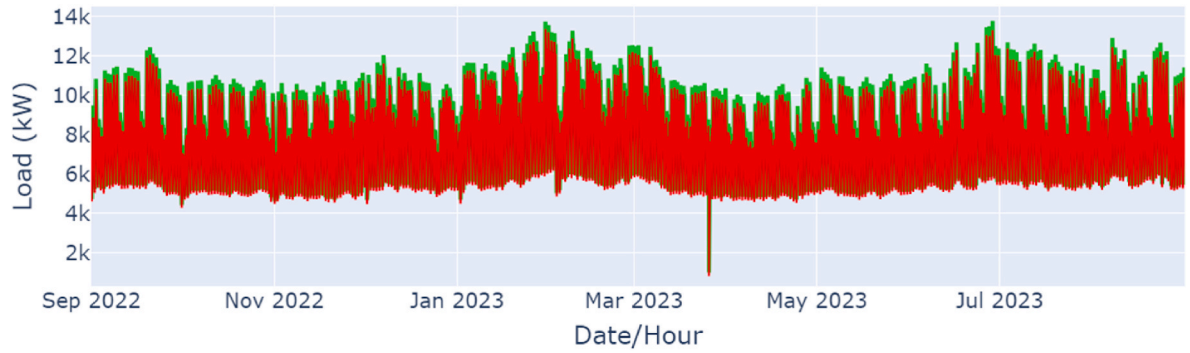


**Fig. 8.** São Ciro substation load diagram with data from the Open Data portal, highlighting the associated EV consumption. The red lines represent scenarios without EV consumption; the green lines represent scenarios with EV consumption. (For interpretation of the references to colour in this figure legend, the reader is referred to the Web version of this article.)

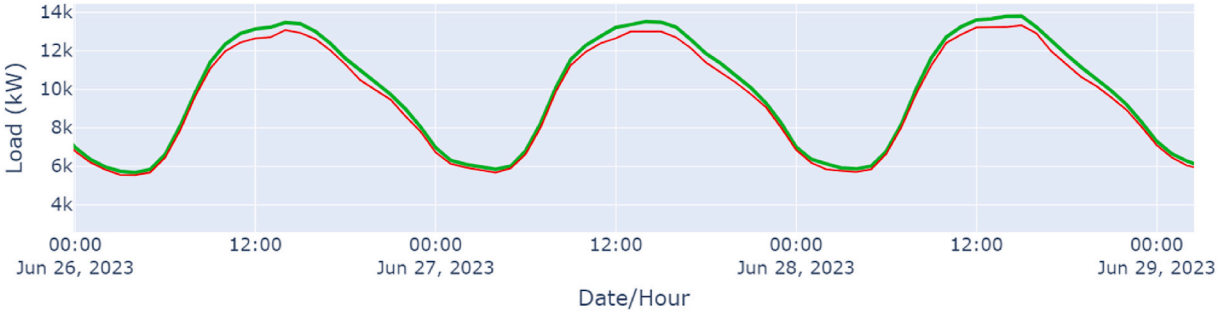


**Fig. 9.** Intraday variation of the São Ciro substation load from June 26 to 29, using data from the Open Data portal, highlighting the associated EV consumption. The red lines represent scenarios without EV consumption; the green lines represent scenarios with EV consumption. (For interpretation of the references to colour in this figure legend, the reader is referred to the Web version of this article.)

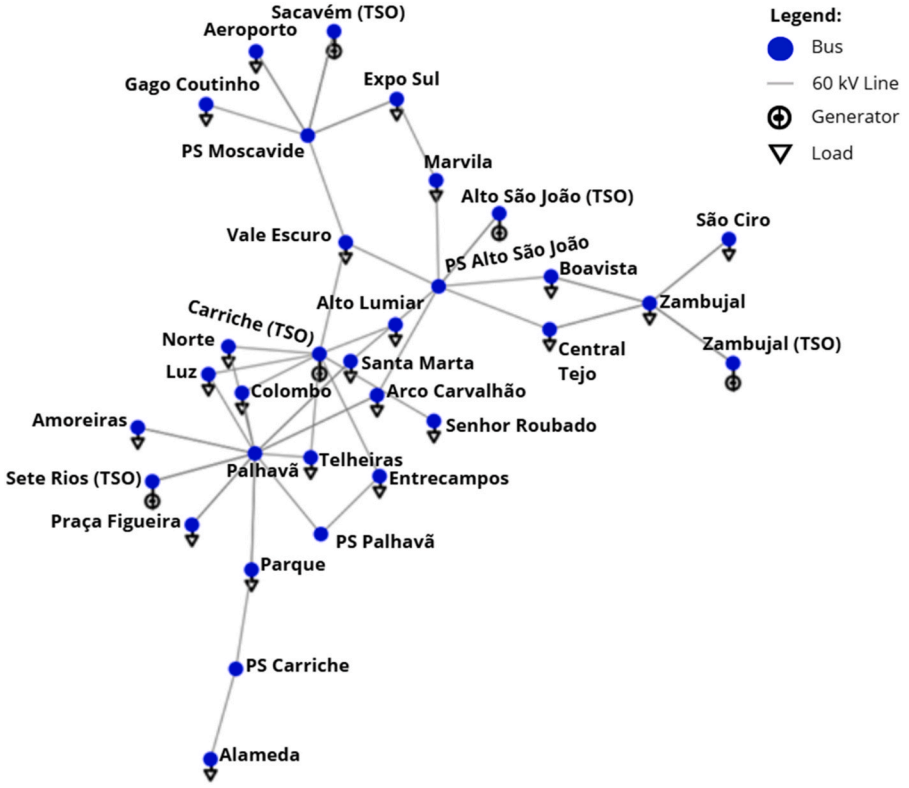


**Fig. 10.** Network model.

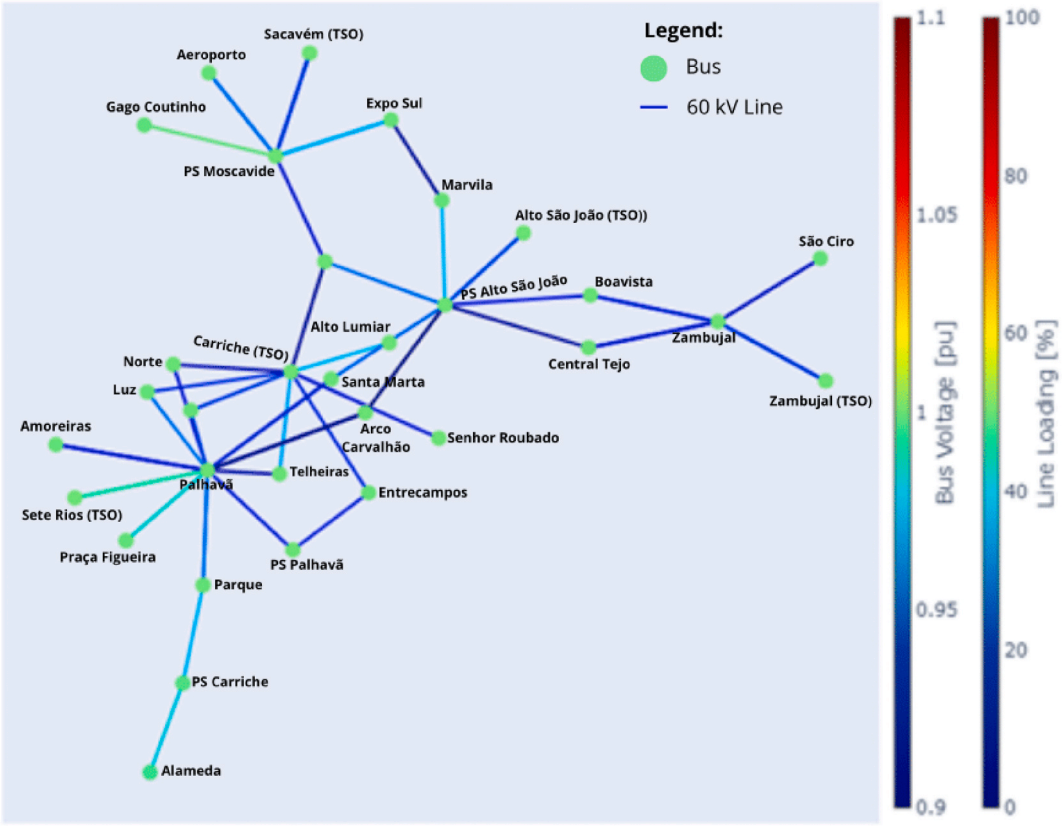


**Fig. 11.** Power flow of the base network on September 30, 2023, at 11:00 p.m., highlighting the voltage levels and percentage line overloads.

For the XHIOLE cable, since specific resistance data for the 1000 mm$^2$ section were not found in the manufacturers' catalogs, the copper resistivity for a specific section per kilometer of cable was determined and used as a reference for the 1000 mm$^2$ section. The resistance of the cables was calculated based on the data provided by the manufacturers, using the DC resistance values at 20 °C and converting them to AC at 75 °C according to Eq. (10). In this equation, $\theta_1$ and $\theta_0$ represent the temperatures, $R(\theta_1)$ and $R(\theta_0)$ are the resistances at temperatures $\theta_1$ and $\theta_0$, respectively, and $\alpha$ is the temperature coefficient of the material.

$$R(\theta_1) = R(\theta_0).\,[1 + \alpha(\theta_1 - \theta_0)] \tag{10}$$

It was assumed that the skin effect was negligible, treating the AC and DC resistance at 75 °C as the same. The inductance and capacitance values were obtained from typical manufacturer data and converted to Ω/km and nF/km, respectively, using a frequency of 50 Hz. Concerning the maximum supported current, in cases where the values were not specified in the E-REDES document, the manufacturer's data were used, assuming that all lines are buried.

## 3. Results and analysis

The described methodology has been deployed to evaluate the impact of electric vehicle charging on the electricity grid in Lisbon, as described in Subsection 3.1. The results are presented and analyzed in terms of load diagram validation (Subsection 3.2), improvements in substation load diagrams through the application of a genetic algorithm. (Subsection 3.3), and the analysis of load patterns specific to electric vehicles (Subsection 3.4). Finally, the impact of electric vehicle charging on the electricity distribution network in Lisbon is presented in Subsection 3.5.

### 3.1. Case study

This study investigates the impact of electric vehicle charging on 60 kV substations within the Lisbon municipality. We utilized hourly energy consumption data for the postal codes collected from the E-REDES Open Data portal, which covers 365 days from September 2022 to August 2023. Electric vehicle load profiles from 2023 were sourced from the MOBI.E network, and grid line characteristics were obtained from E-REDES documentation. Different scenarios (with EV load increase rates of 5, 10, 15, 20, and 30 times) at the respective substations were simulated to assess the impact on the distribution network, focusing on the overloading of grid lines, line losses, and voltage levels at the buses.

### 3.2. Results of substation load diagrams validation

In this subsection, two examples of load diagrams are presented in Figs. 3 and 4, derived from both the Open Data portal of E-REDES and the reference data from E-REDES, but displayed simultaneously.

On the one hand, a visual discrepancy can be observed between the reference data and the data obtained through the geographic distance algorithm for the São Ciro substation. This difference may be attributed to previously mentioned sources of uncertainty, such as the lack of active energy consumption data for particular postal codes or the need for adjustments due to the differing temporal resolutions of the data from both sources. The systematic decrease in power observed in the load diagrams from the Open Data portal coincides with the transition to daylight saving time. During this transition, clocks are advanced from 01:00 a.m. to 02:00 a.m. local time, shifting from Western European Time (WET, UTC+0) to Western European Summer Time (WEST, UTC+1), resulting in significantly lower energy consumption values provided by the Open Data portal at this time compared to the rest. Additionally, it should be noted that the data provided by the portal are approximations of the values extracted from the system, which may

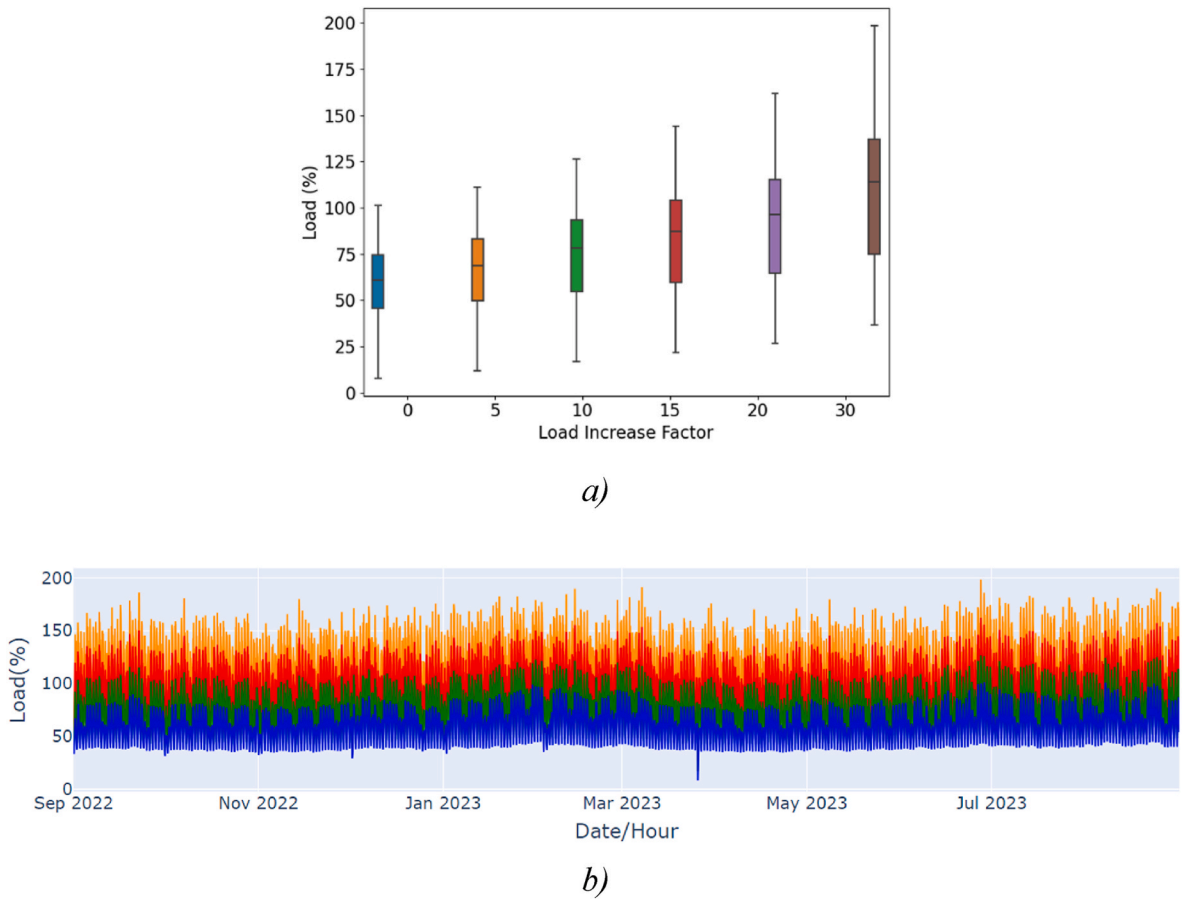


**Fig. 12.** Overload of the Sete Rios - Palhavã 1 line as a result of increasing EV load. a) Load boxplot. b) Load diagram. The blue line represents 0x, the green line represents 10x, the red line represents 20x, and the orange line represents 30x. (For interpretation of the references to colour in this figure legend, the reader is referred to the Web version of this article.)

contribute to the observed variations.

On the other hand, when analyzing the Vale Escuro substation, the results obtained by the first approach used are more favorable and closer to the reference data compared to São Ciro, as there is a less pronounced variation in load profiles and consumption peaks. This similarity between consumption profiles suggests that the geographic distance algorithm proved more suitable for allocating postal code weights to certain substations over others, as shown in Table 3.

### 3.3. Substation load diagram improvements using a genetic algorithm

The variation in load patterns and consumption peaks, along with the RMSE values presented in Table 3 for the geographic distance algorithm, indicated that further adjustments or refinements were required to improve the distribution of postal code weights across substations and, consequently, the load distribution. When the method for improving load diagrams was applied, the results showed significant progress, as illustrated in Fig. 5 and Table 3.

Comparing the load diagram of the São Ciro substation from the previous subsection with the one obtained after applying the genetic algorithm, it is clear that the load profile improved substantially, leading to greater accuracy in postal code weight distribution and enhanced reliability of the data. A notable reduction in variability and discrepancies relative to the reference data was observed, indicating more accurate modeling of the substation consumption profiles.

For the Vale Escuro substation, as shown in Fig. 6, the improvements in load profiles were less pronounced, indicating that the geographic distance algorithm had already performed adequately. Moreover, as discussed in Subsection 2.3.2, several mutation rates were tested to identify the most effective in reducing RMSE for each substation, as shown in Table 3. The average RMSE values for all substations were calculated, along with the percentage reduction in RMSE between the geographic distance algorithm and the genetic algorithm with a 100 % mutation rate.

The analysis of RMSE values across different substations reveals significant improvements after applying the genetic algorithm with various mutation rates. Based on individual and average RMSE reductions, the 100 % mutation rate proved to be the most effective, yielding the lowest RMSE values. Most substations, such as Alto Lumiar, Expo Sul, and São Ciro, experienced substantial reductions in RMSE, as indicated by the percentage improvements in the last column of the table, and none of the substations exhibited worse results after the application of the algorithm. However, substations such as Norte, Senhor Roubado, and Zambujal demonstrated moderate improvements, suggesting that the algorithm had a more limited impact on improving the load profiles of these substations, which are more affected by uncertainty sources. Due to the stochastic nature of the problem, metaheuristics such as genetic algorithms can lead to suboptimal solutions. Therefore, multiple simulations with a 100 % mutation rate were performed, with Table 3 presenting the best result obtained for this rate. As a result, the effect of the uncertainty sources, discussed in Subsection 2.1, was mitigated, allowing for the generation of realistic load diagrams for the substations considered based on postal code-level data from the Open Data portal.

### 3.4. Analysis of electric vehicle load diagrams

For modeling electric vehicle load diagrams, actual data from the

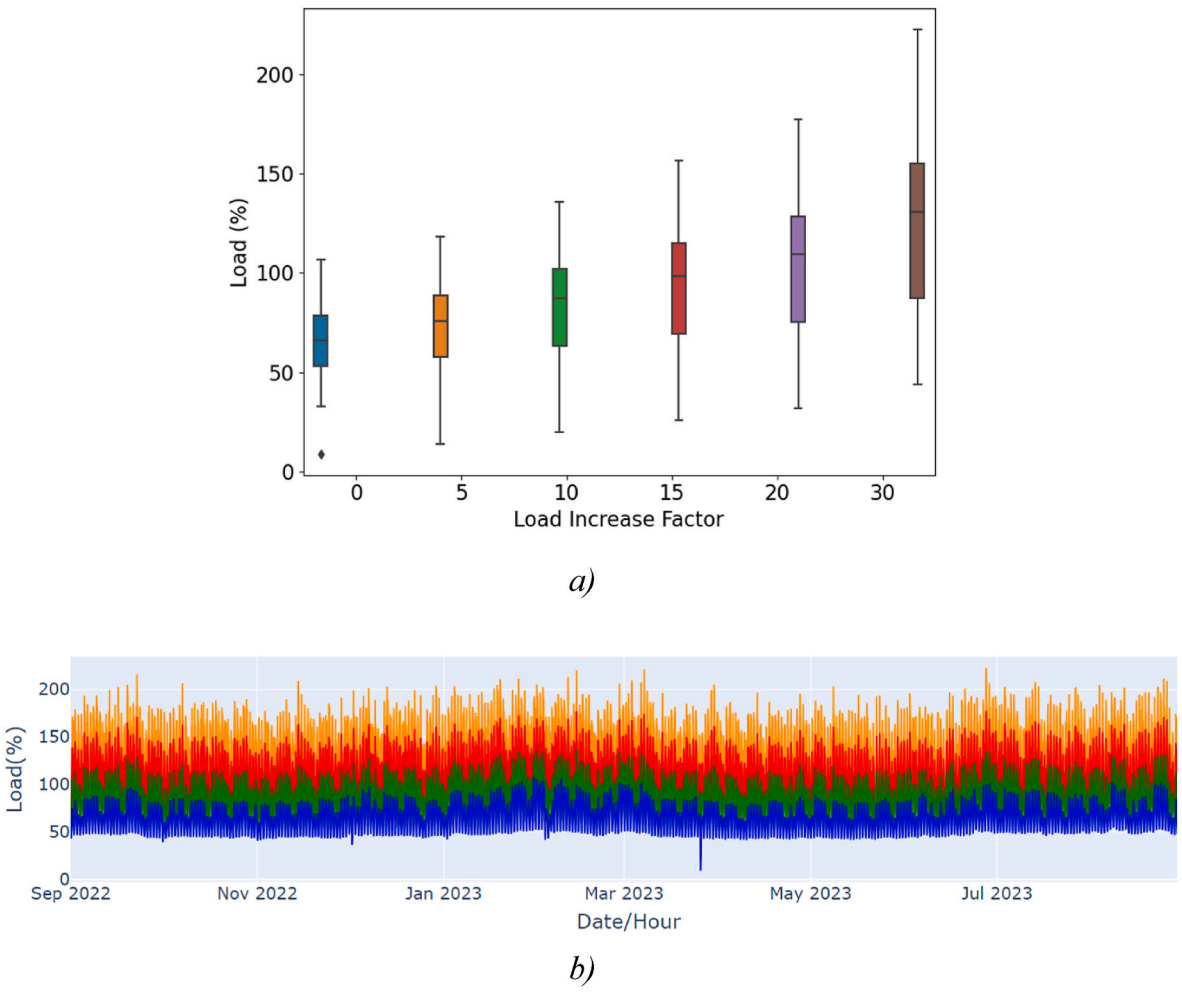


**Fig. 13.** Overload of the PS Moscavide - Gago Coutinho line as a result of increasing EV load. a) Load boxplot. b) Load diagram. The blue line represents 0x, the green line represents 10x, the red line represents 20x, and the orange line represents 30x. (For interpretation of the references to colour in this figure legend, the reader is referred to the Web version of this article.)

MOBI.E network were used to determine the average number of charging points utilized per day within the Lisbon municipality during the study period. Fig. 7 illustrates an example of the power consumption results over 24 h in a specific month. This example was generated from a selection of 30 representative simulations, chosen from a total of 395 simulations conducted for the Lisbon municipality. Each line represents a daily simulation, revealing significant variation in power consumption throughout the day, with pronounced peaks during periods of high activity, reflecting the daily variability in EV power demand.

An illustrative example of the load diagram for the São Ciro substation is shown in Fig. 8, specifically highlighting the consumption of electric vehicles. These data refer to the power consumption data by postal code for EVs after applying the postal code weights determined by the genetic algorithm, as described in Section 2.4.

As shown in Fig. 9, which depicts the intraday variation of substation load over three days during the summer, the load pattern is similar to that observed in Fig. 7, with more pronounced peaks during peak hours, particularly around noon, compared to nighttime periods, such as at 03:00 a.m. This behavior suggests that EV charging predominantly occurs during the day, contributing to increased demand during high-consumption hours.

### 3.5. Analysis of the impact of electric vehicle charging on the Lisbon electricity distribution network

Using data from the Open Data portal, the results and analyses of the evaluation of the impact of electric vehicle charging on the Lisbon electricity distribution network are presented, considering the progressive increase in load across the different substations. The network model obtained is shown in Fig. 10, highlighting the substations operated by the Transmission System Operator (TSO).

In Fig. 11, an example of the power flow in the modeled network is presented, illustrating the topology of the nodes and lines that constitute it. It can be observed that both the lines and buses are within acceptable limits.

#### 3.5.1. Line overloads and peak consumption

To compare the load on the lines resulting from increased electric vehicle charging, two examples of the most critical lines in the network are presented in Figs. 12 and 13. For visualization purposes, the load diagrams do not account for all load increase factors in the boxplots.

As EV load increases at substations, power flow in the lines progressively rises, leading to higher overloads. The most critical lines, which experience significant overloading and require more attention, mainly include *PS Moscavide - Gago Coutinho*, *Carriche - Alto Lumiar*, *PS Carriche - Parque*, *PS Carriche - Alameda*, and *Sete Rios - Palhavã*. In some cases, even with relatively low load-raising factors (e.g., five or ten times), peak loads exceeding 100 % were observed. With a 20-fold increase, half of the load measurements exceeded 80 %, with 25 % of the measurements above 95 %, and some peaks surpassed 130 %. For a 30-fold increase, the situation becomes even more critical, with more than 50 % of the load measurements on some lines exceeding 100 % and peak

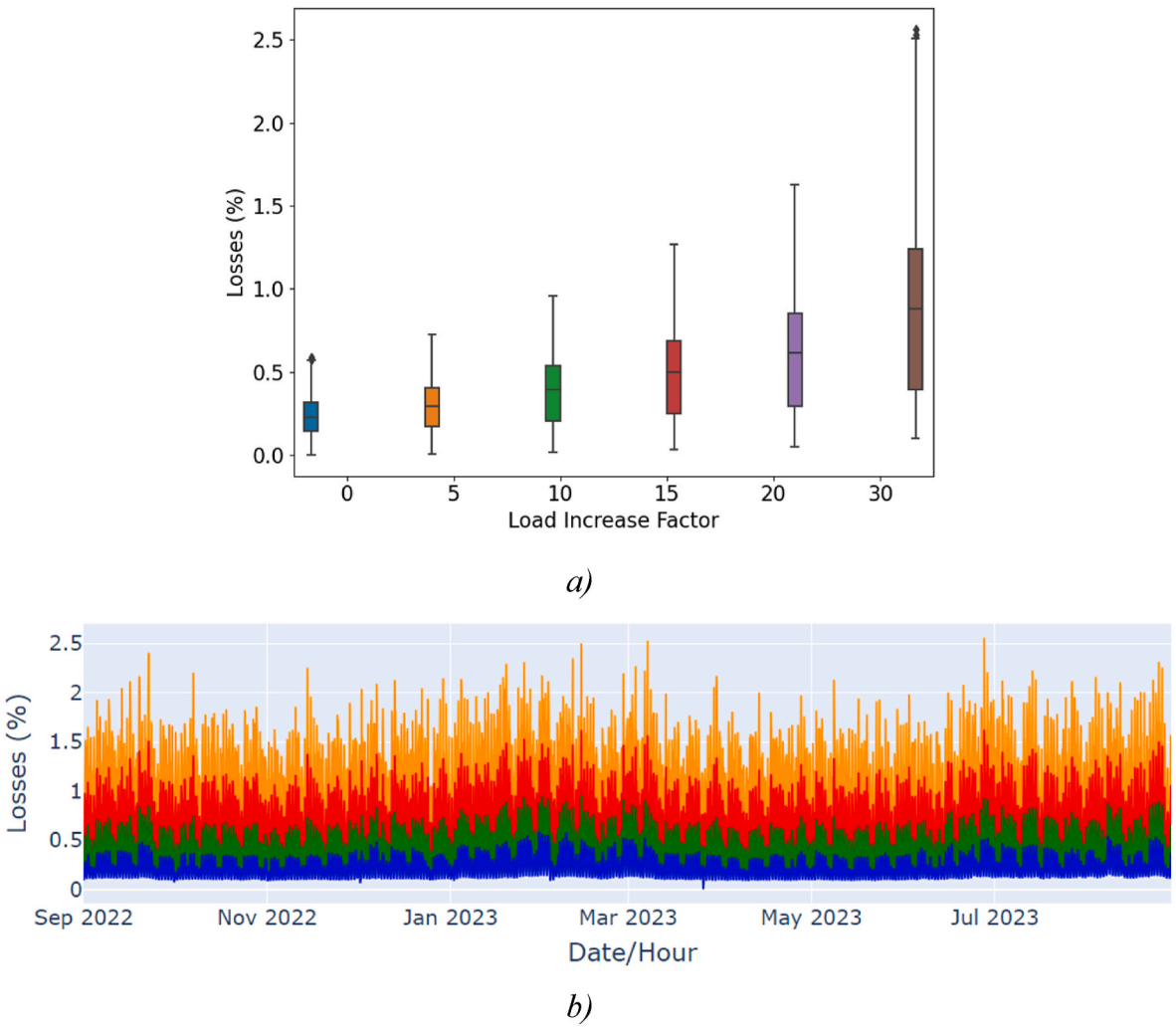


**Fig. 14.** Losses on the PS Moscavide - Gago Coutinho line as a result of increasing EV load. a) Boxplot of losses relative to line capacity. b) Loss diagram relative to line capacity over time. The blue line represents 0x, the green line represents 10x, the red line represents 20x, and the orange line represents 30x. (For interpretation of the references to colour in this figure legend, the reader is referred to the Web version of this article.)

loads reaching values between 161 % and 223 % of the rated capacity. The result is consumption peaks of approximately 50 MW and 40 MW, respectively. Additionally, other lines, although less critical, still require monitoring, such as *PS Moscavide - Expo Sul*, *Carriche - Telheiras*, and *Palhavã - Praça Figueira*, where a 20-fold increase in EV load results in 25 % of the load measurements already exceeding 80 %.

We note that some lines exhibited relatively low load values, indicating operational constraints. Additionally, any outliers in the boxplots represent values outside the expected interquartile range and do not reflect typical network behavior. These arise from consumption peaks during high-demand periods, consumption drops during low-demand periods, or, in some cases, randomly due to occasional variability.

### 3.5.2. Line losses

The same method was applied to evaluate line losses, as shown in Figs. 14 and 15.

The results, presented as a percentage of the line's capacity, indicate that the most overloaded lines do not always have the highest losses since overloading can be temporary, whereas losses are a cumulative process that occurs during the current flow. Additionally, factors such as line length and conductor material resistance play a crucial role in total losses. The analysis shows that as EV load increases at the substations, line losses progressively rise due to the increased current demand from EVs. The lines with the highest losses are primarily *PS Moscavide - Gago Coutinho*, *PS Carriche - Parque*, *PS Carriche - Alameda*, and *Palhavã - Praça Figueira*.

For a 20-fold increase in the *PS Moscavide - Gago Coutinho* line, 25 % of the losses exceed 0.85 %, with maximum values reaching 1.63 %, representing a 185.96 % increase compared to the base scenario. Similarly, for the *PS Carriche-Parque* line, a 10-fold increase results in 25 % of the losses exceeding 0.65 %, with a maximum of 1.17 %. At a 20-fold increase, 50 % of the losses exceed 0.68 %, peaking at 1.81 %. For the *PS Carriche - Alameda* line, a 10-fold increase causes 25 % of the losses to surpass 0.56 %, with a maximum of 1.01 %. At a 20-fold increase, 50 % of the losses exceed 0.58 %, and 25 % exceed 0.83 %, with peaks of 1.55 %. With a 30-fold increase on both lines, 50 % of the losses exceed 0.94 % on the first line and 0.81 % on the second, while 25 % surpass 1.34 % and 1.15 %, with maximum values of 2.64 % and 2.28 %, representing relative increases of 238.46 % and 235.29 %, respectively. For the *Palhavã - Praça Figueira* line, with a 20-fold increase, 25 % of the losses exceed 0.36 %, representing a relative increase of over 83.78 % compared to the base scenario. As with overloading and consumption peaks, outliers are also present in losses, arising for the same reasons previously discussed.

Finally, the overall system losses were analyzed, as shown in Table 4. Even with a 10-fold increase, 25 % of the losses exceeded 4.99 %, representing a 54.35 % relative increase in maximum values compared to the base scenario. For 20-fold and 30-fold increases, the relative increase

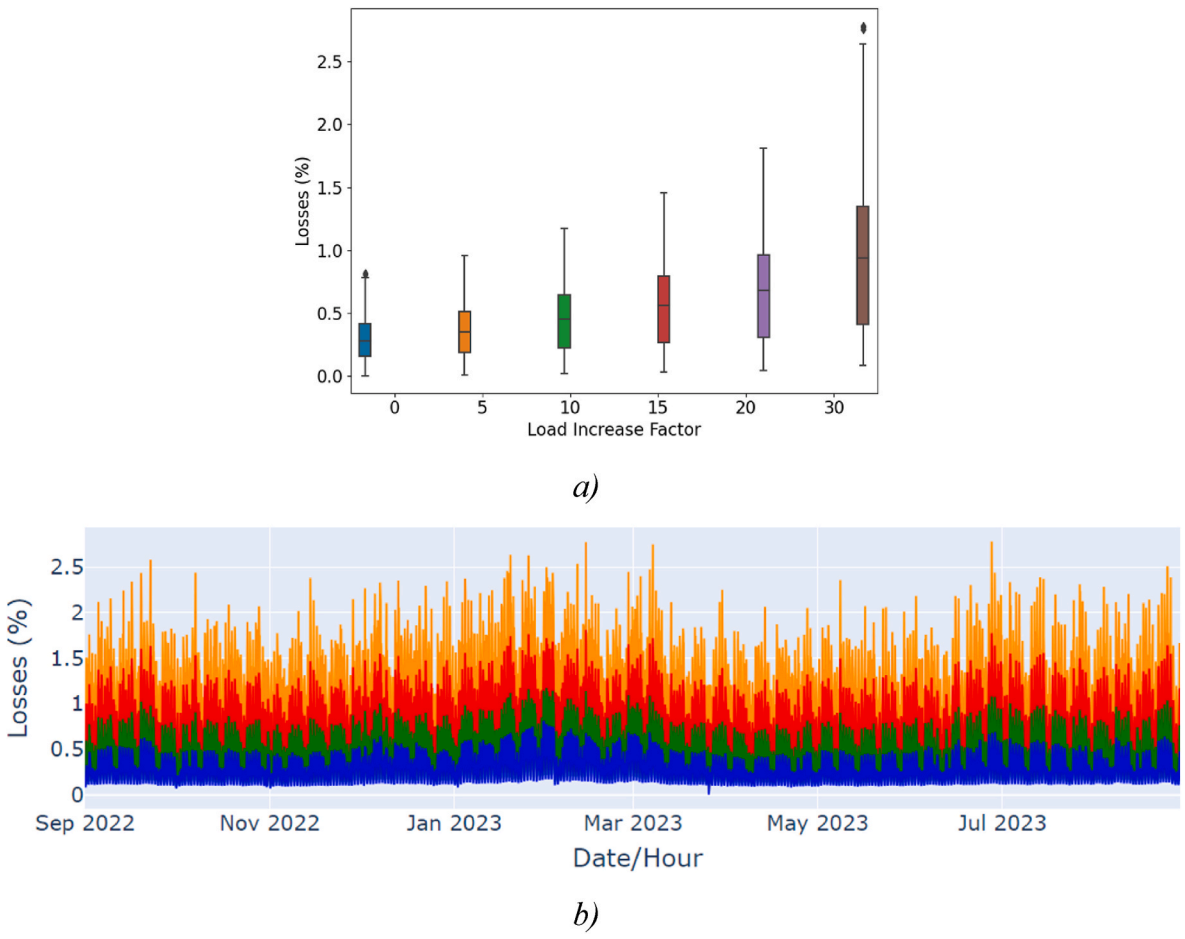


**Fig. 15.** Losses on the PS Carriche - Parque line as a result of increasing *EV load.* a) *Boxplot of losses relative to line capacity*. b) *Loss diagram relative to line capacity over time. The blue line represents 0x, the green line represents 10x, the red line represents 20x, and the orange line represents 30x.* (For interpretation of the references to colour in this figure legend, the reader is referred to the Web version of this article.)

**Table 4**
Descriptive statistics of global losses (%) in the electrical distribution network for different EV load increase factors, using data from the Open Data portal.

| | Factor | Minimum | $Q_1$ | Median | $Q_3$ | Maximum |
|---|---|---|---|---|---|---|
| **Global losses (%) in the electrical distribution network** | 0 | 0.03 | 1.28 | 2.21 | 3.17 | 5.63 |
| | 5 | 0.08 | 1.49 | 2.81 | 3.93 | 6.72 |
| | 10 | 0.16 | 1.80 | 3.60 | 4.99 | 8.69 |
| | 15 | 0.27 | 2.14 | 4.47 | 6.20 | 11.35 |
| | 20 | 0.40 | 2.50 | 5.40 | 7.56 | 14.38 |
| | 30 | 0.76 | 3.30 | 7.56 | 10.70 | 21.08 |

reached significant values of 155.42 % and 274.42 %, respectively.

### *3.5.3. Voltage magnitude at the buses*

An analysis of voltage magnitude variation at the network buses was conducted, considering two scenarios: one without reactive power in the loads and another with reactive power equivalent to 15 % of active power, simulating AC power flow. Some results are presented in Figs. 16 and 17, illustrating two representative examples of the conditions studied.

As the EV load increases, a slight voltage drop is observed at the buses due to the higher current flow, which in turn leads to a larger voltage drop. The introduction of reactive current also results in a minor voltage drop. However, these variations are minimal and can be considered negligible, as network stability is maintained due to sufficient power generation. This approach ensures that voltage remains stable even with significant load variations, providing greater robustness and flexibility to the electrical system.

## 4. Conclusion and future work

This study examines the impact of electric vehicle charging on the electricity distribution network in Lisbon, Portugal, allowing for the assessment of overloads, peak consumption, losses, and voltage variations at the distribution buses. The analysis incorporates real energy consumption data based on postal codes to create specific load profiles for each substation, linking EV consumption to the corresponding postal code areas and substations. This approach enables the modeling of electric vehicle load diagrams. The study also addresses inherent uncertainty by incorporating a genetic algorithm designed to improve substation load diagrams based on both individual and average RMSE. Following the proposed methodology, the current study can also be applied to other distribution networks as long as similar data sources are available.

The results demonstrated that the application of the genetic algorithm led to significant improvements in substation load profiles, improving the average RMSE by up to 36.02 %. The main impacts included a progressive increase in power and current through the lines, resulting in higher overloads and losses. Some lines, even with a load increase factor of just five times, showed overload peaks exceeding 100 %. In more critical scenarios, with a 30-fold increase, load peaks surpassed 161 %, reaching up to 223 %, with 50 % of the loads exceeding 100 % of the lines' capacity. Global system losses also increased

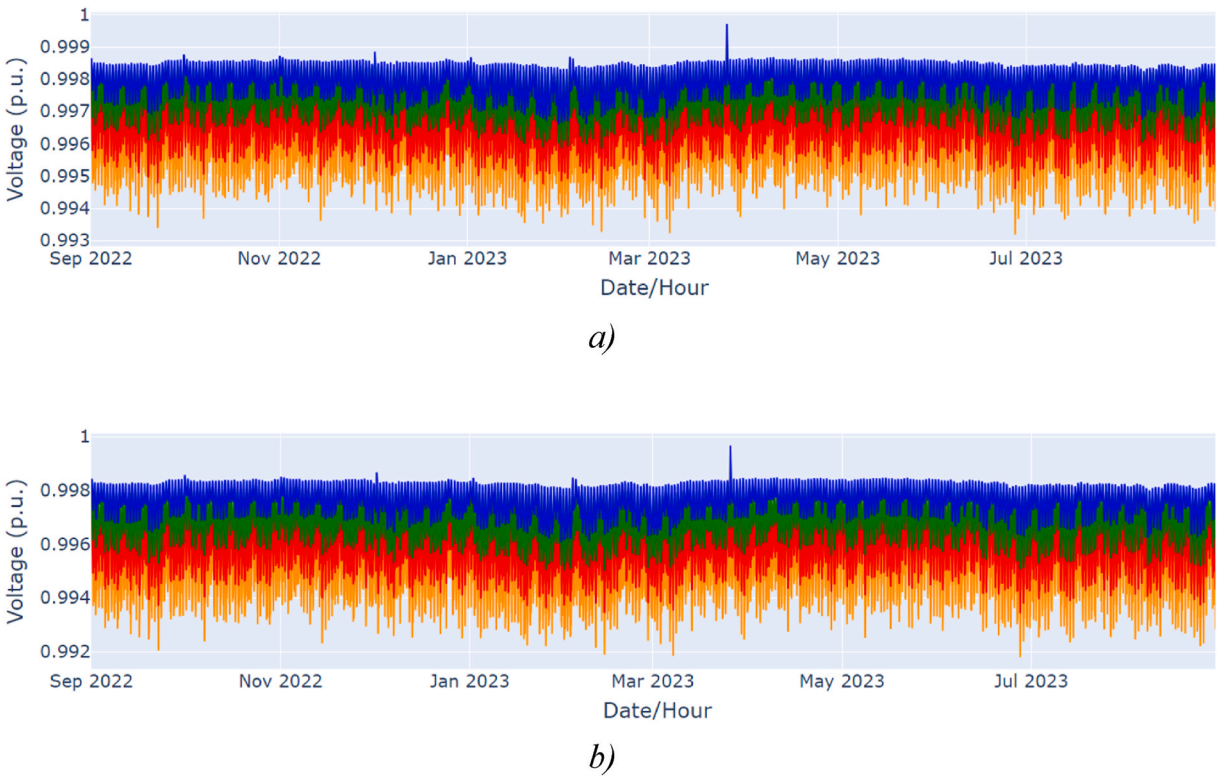


**Fig. 16.** Voltage variation (p.u.) over time at Gago Coutinho as a result of increasing EV load. The blue line represents 0x, the green line represents 10x, the red line represents 20x, and the orange line represents 30x. a) Without reactive power. b) With reactive power (15 % of active power). (For interpretation of the references to colour in this figure legend, the reader is referred to the Web version of this article.)

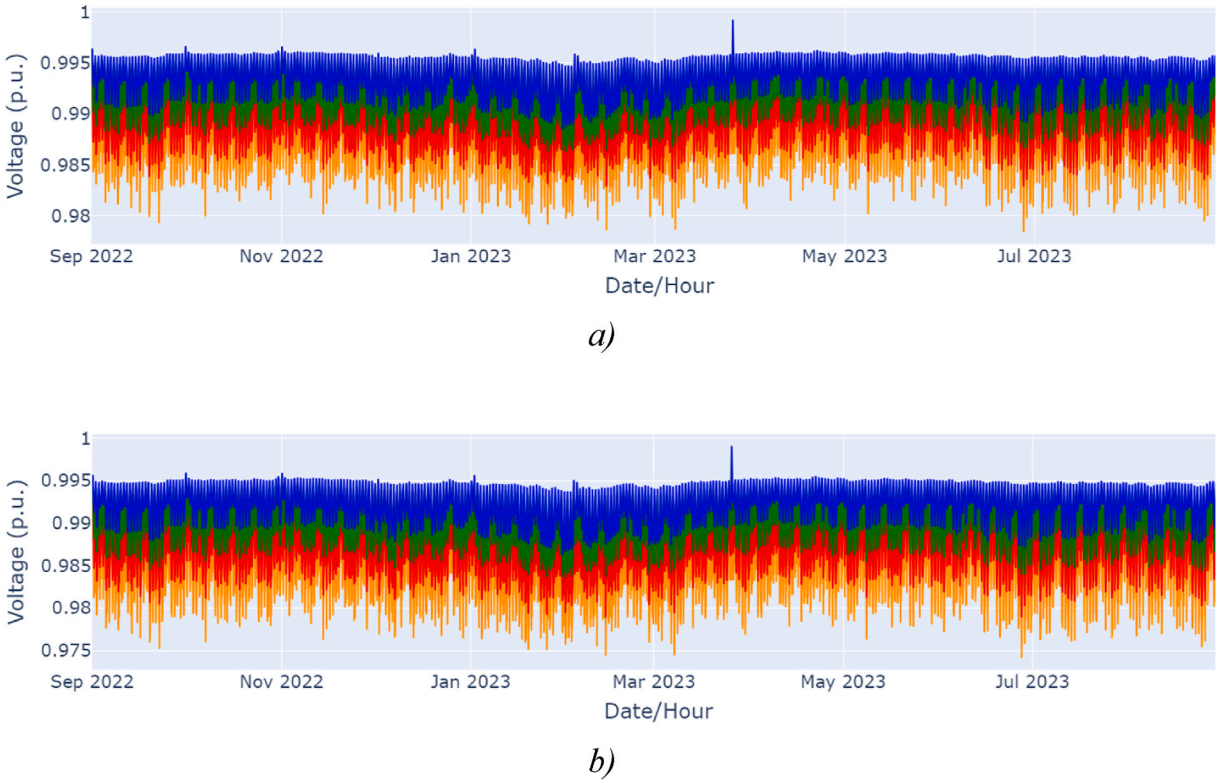


**Fig. 17.** Voltage variation (p.u.) over time at Alameda as a result of increasing EV load. The blue lines are 0x; the green lines are 10x; the red lines are 20x; the orange lines are 30x. a) Without reactive power. b) With reactive power (15 % of active power). (For interpretation of the references to colour in this figure legend, the reader is referred to the Web version of this article.)

significantly, with relative maximum value increases of 155.42 % and 274.42 % for 20 and 30-fold load increases compared to the base scenario. Despite this, the voltage magnitude at the buses remained stable.

Nevertheless, we note that as electric vehicle penetration increases, consumption patterns may shift. However, the genetic algorithm used in this model is adaptable, performing mutations on postal code weights, which allows the model to redistribute loads across substations and maintain the accuracy of the load profiles. With periodic updates based on the most recent data, the model remains robust and well-aligned with evolving consumption trends. Furthermore, the implemented methodology is flexible and can accommodate different levels of EV penetration.

Exploring charging management strategies to reduce grid impacts and consumption peaks represents a future work left open by this study. Additionally, optimizing the integration of renewable energy sources during periods of high production, in conjunction with EV charging, will be considered to minimize grid strain. Finally, assessing the impact of dynamic electricity tariffs on incentivizing off-peak EV charging remains an important avenue for future research.

## CRediT authorship contribution statement

**Miguel Mouquinho Cardinha:** Writing – review & editing, Writing – original draft, Methodology, Investigation. **Rui Amaral Lopes:** Writing – review & editing, Writing – original draft, Methodology, Investigation, Conceptualization. **Nuno Amaro:** Writing – review & editing, Writing – original draft, Methodology, Investigation, Conceptualization.

## Declaration of competing interest

The authors declare that they have no known competing financial interests or personal relationships that could have appeared to influence the work reported in this paper.

## Acknowledgements

This research was partially funded by the Portuguese “Fundação para a Ciência e a Tecnologia” (FCT) in the context of the Center for Technology and Systems (CTS/UNINOVA/FCT/NOVA), reference UIDB/00066/2020.

## Data availability

The authors do not have permission to share data.

## References

Abiassaf, G.A., Arkadan, A.A., 2024. Impact of EV charging, charging speed, and strategy on the distribution grid: a case study. In: IEEE Journal of Emerging and Selected Topics in Industrial Electronics, vol. 5, pp. 531–542. https://doi.org/10.1109/JESTIE.2024.3352505, 2.

Akhavan-Rezai, E., Shaaban, M.F., El-Saadany, E.F., Zidan, A., 2012. Uncoordinated charging impacts of electric vehicles on electric distribution grids: normal and fast charging comparison. In: 2012 IEEE Power and Energy Society General Meeting, pp. 1–7. https://doi.org/10.1109/PESGM.2012.6345583.

Clement-Nyns, K., Haesen, E., Driesen, J., 2010. The impact of charging Plug-In hybrid electric vehicles on a residential distribution grid. IEEE Trans. Power Syst. 25 (1), 371–380. https://doi.org/10.1109/TPWRS.2009.2036481.

Dall-Orsoletta, A., Ferreira, P., Gilson Dranka, G., 2022. Low-carbon technologies and just energy transition: prospects for electric vehicles. Energy Convers. Manag. X 16, 100271. https://doi.org/10.1016/j.ecmx.2022.100271.

Daneshzand, Farzaneh, Coker, Phil J., Potter, Ben, Smith, Stefan T., 2023. “EV smart charging: how tariff selection influences grid stress and carbon reduction“. Appl. Energy 348. https://doi.org/10.1016/j.apenergy.2023.121482.

E-REDES, 2022. “E-REDES - Caracterização Das Redes De Distribuição, Art. 20 do Regulamento De Acesso Às Redes E Às Interligações do Setor Elétrico (In Portuguese),” [Online]. Available: https://www.e-redes.pt/pt-pt/caracterizacao-das-redes-de-distribuicao-3. (Accessed 7 October 2024).

E-REDES - Distribuição de eletricidade. “Portal Open Data E-REDES (in Portuguese).” [Online]. Available: https://e-redes.opendatasoft.com/pages/homepage/. (Accessed 12 January 2024).

European Commission and Directorate-General for Energy, 2019. Clean Energy for all Europeans. Publications Office [Online]. Available: https://data.europa.eu/doi/10.2833/9937. (Accessed 6 January 2024).

European Environment Agency, 2019. The European Environment: State and Outlook 2020: Knowledge for Transition to a Sustainable Europe. Publications Office of the European Union. https://doi.org/10.2800/96749.

Godina, R., Rodrigues, E.M.G., Paterakis, N.G., Erdinc, O., Catalão, J.P.S., 2016. Innovative impact assessment of electric vehicles charging loads on distribution transformers using real data. Energy Convers. Manag. 120, 206–216. https://doi.org/10.1016/j.enconman.2016.04.087.

Hu, X., Chen, N., Wu, N., Yin, B., 2021. The potential impacts of electric vehicles on urban air quality in Shanghai City. Sustainability 13 (2). https://doi.org/10.3390/su13020496.

Instituto Nacional de Estatística, 2023. Estatísticas Ambiente :2022 [Online]. Available: https://www.ine.pt/xurl/pub/439545493. (Accessed 19 January 2024).

JBay Solutions, 2022. “API - Códigos Postais (in Portuguese),” [Online]. Available: https://www.cttcodigopostal.pt/. (Accessed 7 March 2024).

Kumar, B.V., M A, A.F., 2023. A review of technical impact of electrical vehicle charging stations on distribution grid. 2023 International Conference on Recent Advances in Electrical, Electronics & Digital Healthcare Technologies (REEDCON), pp. 559–564. https://doi.org/10.1109/REEDCON57544.2023.10150680. New Delhi, India.

Li, Y., Jenn, A., 2024. Impact of electric vehicle charging demand on power distribution grid congestion. Proc. Natl. Acad. Sci. USA 121 (18), e2317599121. https://doi.org/10.1073/pnas.2317599121.

Lopes, J.A.P., Soares, F.J., Almeida, P.M.R., 2011. Integration of electric vehicles in the electric power system. Proc. IEEE 99 (1), 168–183. https://doi.org/10.1109/JPROC.2010.2066250.

Masoum, A.S., Deilami, S., Moses, P.S., Abu-Siada, A., 2010. Impacts of battery charging rates of Plug-in electric vehicle on smart grid distribution systems. In: 2010 IEEE PES Innovative Smart Grid Technologies Conference Europe. ISGT Europe), pp. 1–6. https://doi.org/10.1109/ISGTEUROPE.2010.5638981.

MOBI.E, “MOBI.Data - MOBI.E.” Accessed: April. 14, 2024. [Online]. Available: https://mobie.pt/mobidata/data.

Nutkani, I., et al., 2024. Impact of EV charging on electrical distribution network and mitigating solutions – a review. IET Smart Grid. 7 (5), 485–502. https://doi.org/10.1049/stg2.12156.

Pieltain Fernández, L., Gomez San Roman, T., Cossent, R., Mateo Domingo, C., Frías, P., 2011. Assessment of the impact of Plug-in electric vehicles on distribution networks. IEEE Trans. Power Syst. 26 (1), 206–213. https://doi.org/10.1109/TPWRS.2010.2049133.

Portuguesa, República, 2019. Plano Nacional Energia E Clima 2021-2030 (PNEC 2030). Portugal, pp. 1–5 (in Portuguese).

Qian, K., Zhou, C., Allan, M., Yuan, Y., 2011. Modeling of load demand due to EV battery charging in distribution systems. IEEE Trans. Power Syst. 26 (2), 802–810. https://doi.org/10.1109/TPWRS.2010.2057456.

Teixeira, A.C.R., Sodré, J.R., 2018. Impacts of replacement of engine powered vehicles by electric vehicles on energy consumption and CO2 emissions. Transp Res D Transp Environ 59, 375–384. https://doi.org/10.1016/j.trd.2018.01.004.

Thurner, L., et al., 2018. Pandapower—an open-source python tool for convenient modeling, analysis, and optimization of electric power systems. IEEE Trans. Power Syst. 33 (6), 6510–6521. https://doi.org/10.1109/TPWRS.2018.2829021.

Ul-Haq, A., Cecati, C., Strunz, K., Abbasi, E., 2015. Impact of electric vehicle charging on voltage unbalance in an urban distribution network. Intell. Ind. Syst. 1 (1), 51–60. https://doi.org/10.1007/s40903-015-0005-x.

Williams, B., Bishop, D., Hooper, G., Chase, J.G., 2024. Driving change: electric vehicle charging behavior and peak loading. Renew. Sustain. Energy Rev. 189 (A). https://doi.org/10.1016/j.rser.2023.113953.